TESTING POINT SOURCE TO LINE SOURCE TRANSFORMATIONS FOR APPLICATION OF FULL WAVEFORM INVERSION TO SHALLOW SEISMIC SURFACE WAVES

M. Schäfer, L. Groos, T. Forbriger, T. Bohlen

email: *M.Schaefer@kit.edu*

keywords: *2D full waveform inversion, geometrical spreading corrections, surface waves*

ABSTRACT

Elastic full waveform inversion (FWI) of shallow seismic surface waves has the potential to reconstruct lateral variations of the shallow subsurface which is important e.g. for geotechnical site characterization. In order to make a 2D full waveform inversion algorithm applicable, shallow seismic field recordings excited by a point source (usually a hammer blow) must be transformed to mimic equivalent wavefields excited by a line source. Waves excited by a point source differ in geometrical spreading, i.e. amplitude decay and phase delay of $\pi/4$ in the far field from waves excited by a line source. In the first part of the report we discuss four different 3D/2D transfomation techniques. One of them use a wave-theoretical approach (Fourier-Bessel expansion) and is exact for 1D subsurface structures. The other transformation techniques are based on the ratio of the Fourier coefficients of the 2D and 3D Green functions for homogeneous fullspace (e.g. Direct Wave Transformation). However, we show that they are applicable to 2D structures. In the second part of the report we investigate reconstruction tests of a 2D subsurface model. We apply the 2D full waveform inversion to line source and corrected point source seismograms as observed data. The FWI to shallow seismic surface waves with line source wavefields can reliably reconstruct the 2D subsurface structure. The Fourier-Bessel Transformation produces strong artifacts due to the 2D characteristic of the subsurface. When using the L2 norm as a measure of misfit a correction for the different decay of amplitudes is mandatory but not sufficient to obtain reliable results. The most appropriate correction filter is the Direct Wave Transformation as it is applicable to 2D structures and single traces and it corrects both the amplitude-decay as well as the phase delay.

INTRODUCTION

The inversion of shallow seismic surface waves is very attractive for geotechnical site investigations. Surface waves which are easily excited by a hammer blow. They have a high sensitivity to the shear wave velocity in the first meters of the subsurface. A hammer blow as a source dominantly excites surface waves and thus the signal to noise ratio of surface waves is very high compared to body waves. With surface waves it is possible to investigate sites with low-velocity zones which cannot be done with refracted body waves. There are established methods to invert surface waves (e. g. inversion of dispersion curves or wavefield spectra (Forbriger, 2003)) but all these methods assume 1D subsurface structures. This assumption is not valid in many applications of practical relevance. To overcome this limitation we want to apply an elastic full waveform inversion (FWI) to shallow seismic surface waves. First successful applications of a FWI to surface waves show the high potential of this method (Romdhane et al. (2011); Tran and McVay (2012)). The application of a 3D FWI to surface waves unfortunately is still difficult due to excessive computational requirements (Dunkl et al., 2012). Therefore we use a 2D inversion developed by Köhn (2011). It is based

on the adjoint method and the forward modeling is done with the Finite Difference method (Bohlen, 2002). Both are applied in the time domain.

With the objective to realize a 2D full waveform inversion of field data, we have to deal with the different spreading of recorded and computed waves. Observed data are commonly gained with a point source such as a hammer blow or an explosion which produces a wavefield with 3D geometrical spreading. However, our inversion-code uses 2D forward modeling and assumes implicitly a line source. Due to unequal decay of amplitudes and a phase shift of $\frac{\pi}{4}$ in the farfield point source and line source wavefields are different. These residuals may result in model artifacts during a full waveform inversion and for this reason we want to investigate the effects of geometrical spreading corrections for a 2D FWI of shallow seismic surface waves. Therefore field data must be preprocessed to simulate the response of a line source. After the point source wavefields are filtered, the wavefields are inverted by a 2D full waveform inversion. A simulation of a line source in the field is to expensive due to a huge number of required shot locations. Therefore we apply different numerical transformations to point source wavefields to simulate line source wavefields. The testing model (Figure 7a)) was inspired from a transverse section of a vertical fault located on the southern rim of the Taunus (near Frankfurt on the Main, Germany). Perpendicular to this fault a shallow seismic measurement have taken place in summer of 2011. The present study is in preparation for inverting this field data record.

The report is organized as follows. To investigate the significance of the different geometrical spreading of line source and point source wavefields, we firstly investigate the accuracy of four different numerical transformations and discuss the waveform fit of corrected point source wavefields with respect to reference wavefields for a line source. We are using on the one hand an exact wave-theoretical approach for 1D subsurface sturctures and on the other hand single-trace transformations. Secondly we use these transformed point source wavefields in a 2D full waveform inversion as observed data to investigate the effects of geometrical spreading corrections for a 2D FWI of shallow seismic surface waves.

3D/2D TRANSFORMATION TECHNIQUES FOR SHALLOW SEISMIC SURFACE WAVES

There are several 3D/2D transformation techniques known from literature. Some of them use a wave-theoretical approach which requires a complete common source gather and other transformation techniques have the benefit to be applicable to single traces. We calculated 3D and 2D wavefields, respectively with a 3D and 2D Finite Difference forward modeling code in the time domain (Bohlen, 2002), on a 2D subsurface structure (see Figure 7a)). With regard to the FWI in the second part of the paper we have used 20 vertical point forces resembling hammer blows and recorded the wavefields with 88 receivers (vertical and horizontal component) with 1 m spacing. We show examplary the vertical component of three shots at 5 m distance (very left part of the model), at 50 m distance (middle of the model) and at 94 m distance (very right part of the model). We have investigated following transformation techniques:

- Transformation 1 - amplitude-only Transformation: scaling with $\sqrt{2\pi r/k}$ in time domain, but no phase transformation,
- Transformation 2 - Fourier-Bessel Transformation: an exact transformation of amplitude and phase for 1D media by using Fourier-Bessel-expansions (e.g., Wapenaar et al. (1992)),
- Transformation 3 - Direct Wave Transformation: spreading correction by convolution with $t^{-1/2}$ in Fourier domain, taper with $t^{-1/2}$ and scale with offset r in time domain (Forbriger et al., 2012),
- Transformation 4 - Single Velocity Transformation: multiplication with $\sqrt{2\pi r/k} \cdot e^{i\pi/4}$ in Fourier domain (Forbriger et al., 2012).

Transformation 1 - amplitude-only Transformation

In a first step it is quite interesting to use hardly any correction. However, the amplitude-decay of waves excited by a point and a line source differ strongly. When we use the L2 norm as a measure of misfit during the inversion, true amplitudes are taken into account and therefore we have to correct the different amplitude-decay with offset. To obtain an offset dependent correction factor we take the ratio of Green's

functions $g_k^{2D}(r)$ and $g_k^{3D}(r)$ for the acoustic wave equation in 2D and 3D after Forbriger et al. (2012), respectively,

$$\frac{g_k^{2D}(r)}{g_k^{3D}(r)} \approx \sqrt{\frac{2\pi r}{k}} \cdot e^{i\pi/4}, \tag{1}$$

with $k = \omega/\alpha$ is the wavenumber, α the phase velocity of the wave, ω the angluar frequency and r is the distance to the source. Thereby we can divide the first factor in two parts: $\sqrt{r}$ accounts for the geometrical spreading and $\sqrt{2\pi/k}$ for the different energy-level of 2D and 3D wavefields. The second factor $e^{i\pi/4}$ indicates that waves excited by a point source differ in a phase delay of $\pi/4$ in the far field from waves excited by a line source. With Transformation 1 we only apply an amplitude correction. Therefore we multiply the traces of the point source wavefields with $\sqrt{2\pi r/k}$ to fit the energy-level and correct geometrical spreading. An appropriate wavenumber k has to be approximated e.g. from an analysis of Fourier-Bessel-expansion coefficients. For this example we have choosen a wavenumber $k = 2\pi$ 30Hz / $280\frac{\text{m}}{\text{s}} = 0.67\frac{1}{\text{m}}$. With this approach it is possible to fit the energy-level and the amplitude-decay with offset. The amplitude discrepancy between seismograms excited by a line and a point source and the enhancement of Transformation 1 is illustrated in Figure 2, in which the normalized RMS amplitude values of a line source seismogram, a point source seismogram and a corrected point source seismogram with Transformation 1 have been computed and plotted as a function of the source to receiver offset r. It is quite surprising that such a simple spreading correction fits the different geometrical spreading of point and line source wavefields. Comparison of line source and amplitude-only corrected point source seismograms of the three exemplary shots are plotted in Figure 1. We observe a good fit of the amplitude-decay of seismograms excited by a line and a point source with Transformation 1. Still there are significant phase residuals over the whole offset range. In Figure 1a) we observe in the near offset range (0-40 m, 0-0.2 s) direct surface waves which correspond to the 1D structure in the left part of the subsurface model. With larger offset (40-80 m, 0.2-0.5 s) we notice a change in the dispersion of the direct surface waves due to the thinner layer in the right part of the subsurface model. We also see reflected surface waves (0-40 m, 0.2-0.5 s) resulting from the step of the layer which reveal on the 2D charateristic of the subsurface model.

Transformation 2 - Fourier-Bessel Transformation

Here we apply a transformation of amplitude and phase for 1D media suggested by Wapenaar et al. (1992) and Amundsen and Reitan (1994) which is exact for 1D structure. Given a vertical point force as a source in the origin of the coordinate system and a receiver profile along the horizontal y-axis. For 1D media we can use a Fourier-Bessel-expansion to express the vertical component of the wavefield at offset r by

$$\tilde{u}_P(r,\omega) = \int_0^\infty G(\omega,p) J_0(\omega p r) \omega^2 p dp \tag{2}$$

with the Fourier transform $\tilde{u}_P$ of the excited wavefield, the expansion coefficients G, the slowness p, the source to receiver distance r, the Bessel function J_0 of order zero and the angular frequency ω. The seismograms of a line source in a distance y to the line source can be written as a superposition of seismograms excited by an infinite number of point sources along the x-axis. Therefore we obtain

$$\tilde{u}_L(y,\omega) = \int_{-\infty}^\infty \tilde{u}_P(\sqrt{x^2+y^2},\omega) \frac{dx}{[x]} \tag{3}$$

for the Fourier coefficients of a seismogram $\tilde{u}_L(y,\omega)$ excited by a line source along the x-axis. Inserting equation (2) into equation (3) we obtain after some calculation steps

$$\tilde{u}_L(y,\omega) = 2\int_0^\infty G(\omega,p)\cos(\omega p y)\omega dp \tag{4}$$

for the line source seismograms. Summarizing this transformation we first have to calculate the expansion coefficients G from the point source seismograms by the back transformation of equation (2) via

$$G(\omega,p) = \int_0^\infty \tilde{u}_p(r,\omega) J_0(\omega p r) r dr. \tag{5}$$

Afterwards we have to do an expansion with plane waves according to equation (4). The transformation for the radial component can be derived in an analog way.

Transformation 2 is indeed exact for 1D media (model changes only in depth) but we apply it in this case to waves on a 2D structure (lateral heterogeneity). Comparison of line source and corrected point source seismograms with Transformation 2 are plotted in Figure 3. For a shot at 5 m distance in Figure 7a) the transformation works quite well for the direct surface waves that correspond to the 1D structures in the left and right part of the subsurface model. However, Transformation 2 neither reproduces amplitudes nor phases of the reflected surface waves as this transformation is only valid for 1D media and therefore cannot explain backpropagating waves. Moreover there is an artefact generated (see Figure 3a)) between 0-40 m and 0.18-0.25 s) which propagates with a very high velocity and interferes with the actual signal. Seismograms of a shot at 50 m distance (middle of the subsurface model) are plotted in Figure 3b). This shot is located on the fault in the subsurface model and produce a significant different dispersion to the left and to the right of the shot location. Anyway, Transformation 2 calculates a kind of pseudo 1D medium and has not the ability to explain the different dispersion in the left and right part of the model. We can clearly observe this behaviour in Figure 3b). Waves for a shot in the right part of the model (Figure 3c)) do not contain strong 2D charateristics. The transformation performs quite well in this case.

Transformation 3 - Direct Wave Transformation

The wave-theoretical approach is limited to 1D structures and cannot handle laterally heterogeneous structures. In reflection seismics a single-trace transformation has been suggested by Pica et al. (1990) and Crase et al. (1990) which is commonly applied for body waves. Forbriger et al. (2012) suggest a slightly different approach. The conversion factor of eq. 1 can be factorized to

$$\sqrt{\frac{2\pi r}{k}} \cdot e^{i\pi/4} = r \cdot \sqrt{\frac{1}{t}} \cdot \sqrt{\frac{\pi}{|\omega|}}(1 + \mathrm{i}\,\mathrm{sign}(\omega)), \tag{6}$$

with $k\alpha = \omega$, where α is the phase velocity of the wave. t is the travel time of a wave travelling with velocity α over a distance of r. The first factor accounts for geometrical spreading of the waves, the second factor is applied by tapering the time series and the third factor is applied in the Fourier domain and equals a convolution with $t^{-1/2}$ in the time domain. This correction is called Direct Wave Transformation, because we assume that the wave travel path equals the source to receiver offset r. Comparison of line source and corrected point source seismograms with Transformation 3 are plotted in Figure 4. The transformation is quite accurate for all shot locations on the subsurface model. The phases of the direct and the reflected surface waves are corrected. Even the amplitudes are fitted appropriately for the direct surface waves. However, the amplitudes of the reflected surface waves are rather too small due to the $t^{-1/2}$ taper. This transformation corrects both the phases and the amplitudes and does not require any a priori information. Furthermore, it is applicable to single traces and for 2D structures.

Transformation 4 - Single Velocity Transformation

We have tried different ways to implement eq. 1. Another approach with a constraint is the assumption of one single phase velocity. This way we can directly divide the Fourier transform $\tilde{u}_P(r,\omega)$ of a wavefield excited by a point source by the Fourier transform of the 3D Greens function and multiply by the 2D Greens function. We obtain a Fourier transform $\tilde{u}_L(r,\omega)$ of the far-field excited by a line source

$$\tilde{u}_L(r,\omega) \approx \tilde{u}_P(r,\omega)\frac{g_k^{2D}(r)}{g_k^{3D}(r)} \tag{7}$$

$$\tilde{u}_L(r,\omega) \approx \tilde{u}_P(r,\omega)\sqrt{\frac{2\pi r}{k}} \cdot e^{i\pi/4} \tag{8}$$

where k is the wavenumber and r is the source/receiver offset. The selection of one single phase velocity is only appropriate for the impulse response in homogenous full space. Our true subsurface model is for sure no homogenous full space, but a 2D structure on a halfspace with free surface. So it is quite interesting how far we can push such a simple transformation and it works really well for this example. To obtain

the single wave velocity we have picked travel times of the near offset traces for the shot at 5 m distance. We have choosen 280 m/s for the single wave velocity for this example. Comparison of line source and corrected point source seismograms with Transformation 4 are plotted in Figure 5. The Single Velocity Transformation is quite accurate for all shot locations on the subsurface model. In comparison with the Direct Wave Transformation it is conspicuous that the amplitude fit of the shot at 5 m distance for the near offset traces is significantly better for the Single Velocity Transformation. The mistake due to the assumption of a single phase velocity is obvisouly rather small in this case. However, we have investigated this correction filter only for this case study. So this assumption could cause artifacts in more complex subsurfaces.

Discussion - 3D/2D transformation techniques

We have introduced four 3D/2D transformation techniques. We have applied these transformations to all 20 shots over the whole range of the subsurface model and calculated for every single shot the L2 norm between the line source reference seismograms and the corrected point source seismograms. Figure 6 displays the individual L2 norm misfit, which is normalized to the energy of the line source seismograms, over the shot location.

Transformation 1 is an amplitude-only transformation (scaling with $\sqrt{2\pi r/k}$) which is mandatory due to the misfit definition with the L2 norm. This transformation produces a more mor less constant L2 value of approximately 56 % over all shot locations. The large misfit is produced by the signifcant phase mismatch over the whole offset range.

Transformation 2 uses a wave-theoretical approach and is only valid for 1D media but we apply it in this example to waves on a 2D structure. When we give a closer look to Figure 6 we see a charateristic misfit trend with the shot locations which corresponds very similar to changes in the subsurface model. For the shot locations in the left part of the subsurface model the L2 norm misfit is about 19 % although Transformation 2 corrects the phases and the amplitudes. However, the reflected surface waves which correspond to the 2D charateristic of the model cannot be reproduced, they even produce strong artifacts. The L2 norm misfit increases (up to 48 %) in the middle of the subsurface model in the area of the step in the layer. A shot exactly on the fault would produce a significantly different dispersion to the left and right part of the model. Anyway, Transformation 2 produces waves for a kind of pseudo 1D medium and has not the ability to explain the different disperion in the left and right part of the model. Shots in the right part of model don't contain strong 2D charateristics why the L2 norm misfit decreases to about 8 %.

Transformation 3 corrects the phase by convolution with $t^{-1/2}$ and additionally the traces are tapered with $t^{-1/2}$ and scaled with source to receiver offset r. The phase and amplitude correction reduce the misfit of line source and point source seismograms remarkable and produce L2 value of about 19 % for all shot locations. This rather high value is due to the taper of $t^{-1/2}$ which produce the amplitudes of near offset traces too small.

Transformation 4 is completely done in the frequency domain by applying eq. 8. This approach works only for waves of a single given wave velocity. Our choosen wave velocity of 280 m/s is obtained from the seismograms and yields to a good fit of line source and corrected point source seismograms. Even the amplitude fit of near offset traces is accurate due to the fact that we don't have to apply the $t^{-1/2}$-taper. The L2 value amounts to about 11 % for all shot locations.

We have to keep in mind that for this example with synthetic data the true line source response is known. We should think about a transformation which is most independent and appropriate for applying for field data later on. Therefore, it would be quite counterproductive to choose a 3D/2D correction like Transformation 2 (Fourier-Bessel) which is only valid for 1D media. From our point of view Transformation 3 appears to be the most appropriate 3D/2D transformation technique for surface waves. The good performance of the Single Velocity Transformation results probably from the narrow bandwidth of the seismic data.

In the second part of the report we use these transformed point source seismograms in a 2D full waveform inversion as observed data and investigate the effects of the different geometrical spreading corrections for shallow seismic surface waves during a full waveform inversion.

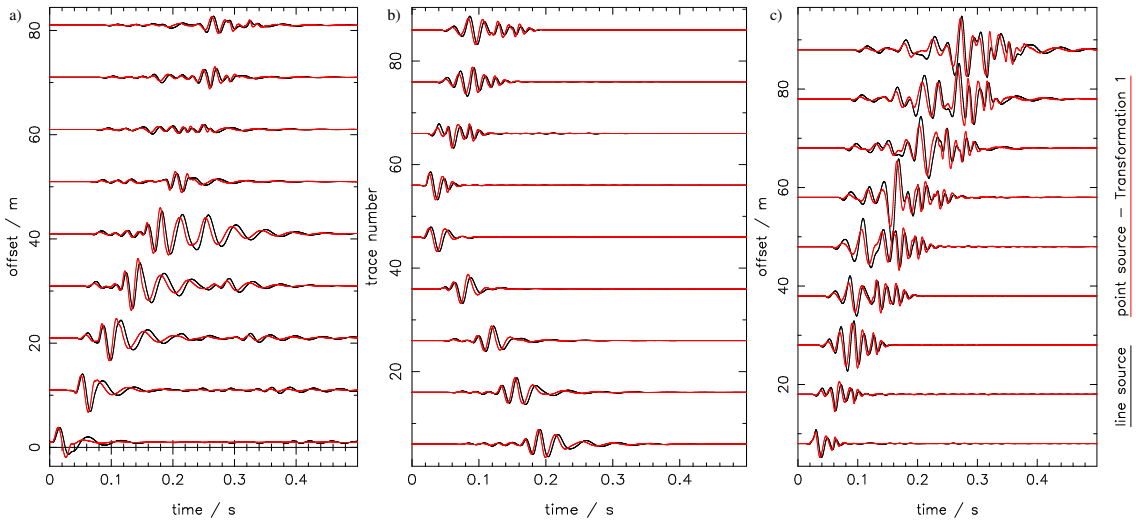

Figure 1: Transformation 1 - amplitude-only Transformation. Comparison of line source seismograms (black) and corrected point source seismograms (red) (vertical component) for the true model in Figure 7a); not all traces are shown. Seismogram a) shows a shot at 5 m distance (very left part of the model), seismogram b) a shot at 50 m distance (middle of the model) and seismogram c) a shot at 94 m distance (very right part of the model). The seismograms in a) and c) are not trace normalized but scaled by an offset dependent factor $\left(\frac{r}{1\,\mathrm{m}}\right)^{0.3}$ to equalize plot scale amplitudes. The seismogram b) is trace normalized, please notice that the y-axis is the trace number not the offset in this case.

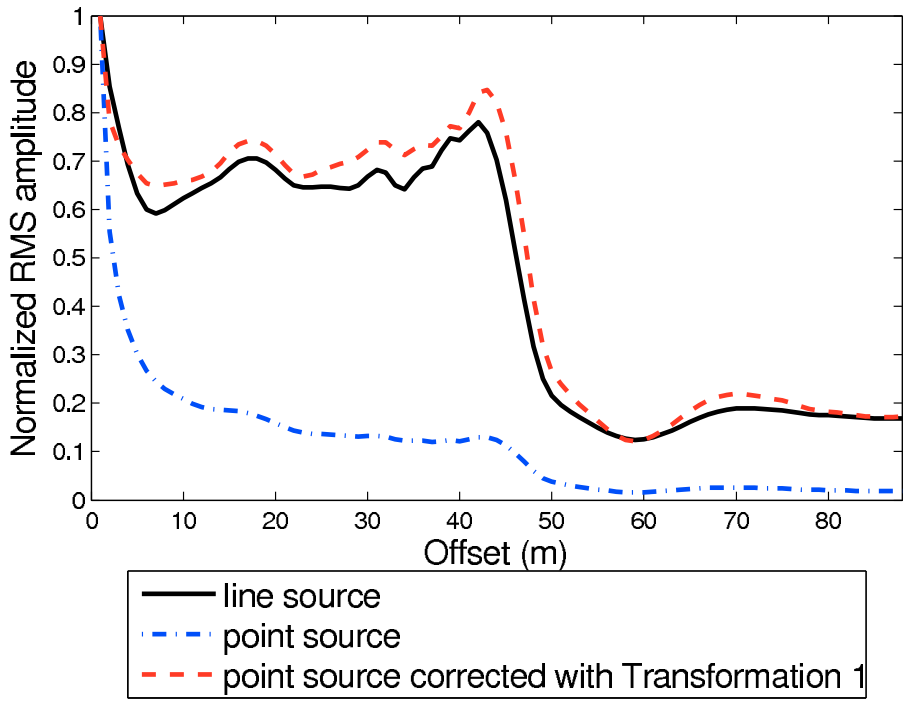

Figure 2: RMS amplitudes of wavefields from a shot at 5 m distance versus source-receiver offset from a line source (solid curve), compared with a point source (dash-dotted curve) and a point source which is corrected with Transformation 1 (dashed curve).

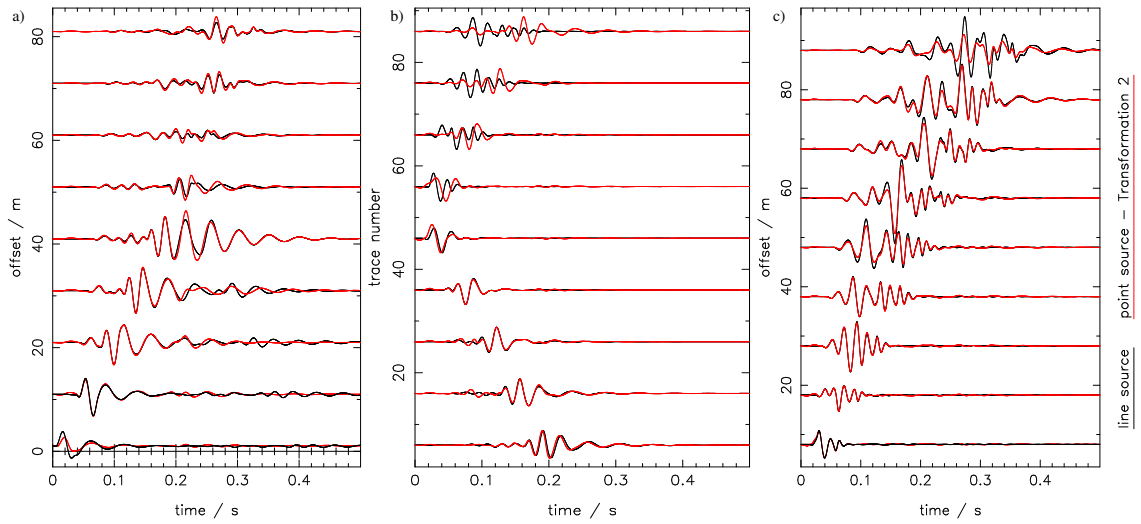

Figure 3: Transformation 2 - Fourier-Bessel Transformation. Comparison of line source seismograms (black) and corrected point source seismograms (red) (vertical component) for the true model in Figure 7a); not all traces are shown. Seismogram a) shows a shot at 5 m distance (very left part of the model), seismogram b) a shot at 50 m distance (middle of the model) and seismogram c) a shot at 94 m distance (very right part of the model). The seismograms in a) and c) are not trace normalized but scaled by an offset dependent factor $\left(\frac{r}{1\,\mathrm{m}}\right)^{0.3}$ to equalize plot scale amplitudes. The seismogram b) is trace normalized, please notice that the y-axis is the trace number not the offset in this case.

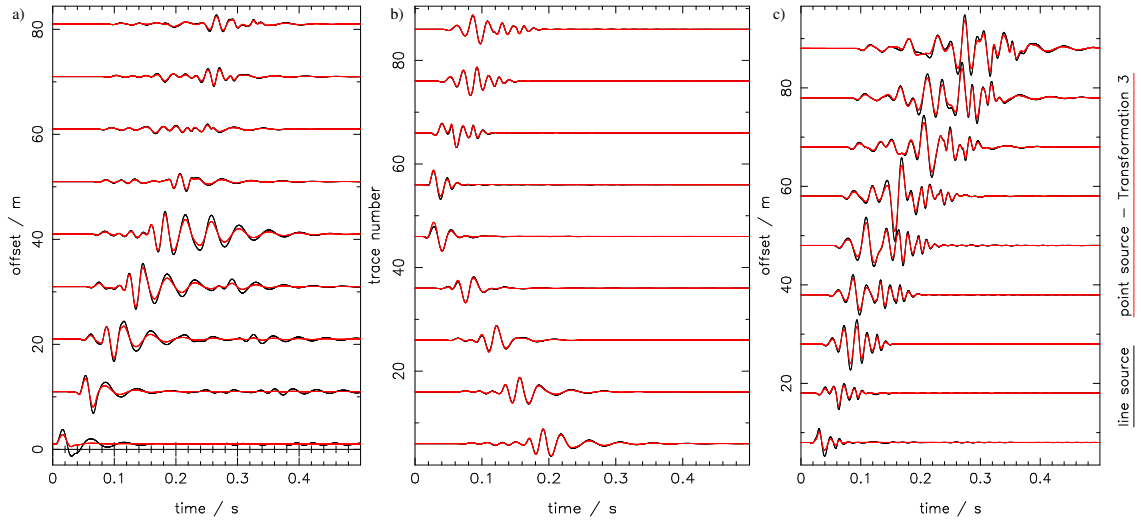

Figure 4: Transformation 3 - Direct Wave Transformation. Comparison of line source seismograms (black) and corrected point source seismograms (red) (vertical component) for the true model in Figure 7a); not all traces are shown. Seismogram a) shows a shot at 5 m distance (very left part of the model), seismogram b) a shot at 50 m distance (middle of the model) and seismogram c) a shot at 94 m distance (very right part of the model). The seismograms in a) and c) are not trace normalized but scaled by an offset dependent factor $\left(\frac{r}{1\,\mathrm{m}}\right)^{0.3}$ to equalize plot scale amplitudes. The seismogram b) is trace normalized, please notice that the y-axis is the trace number not the offset in this case.

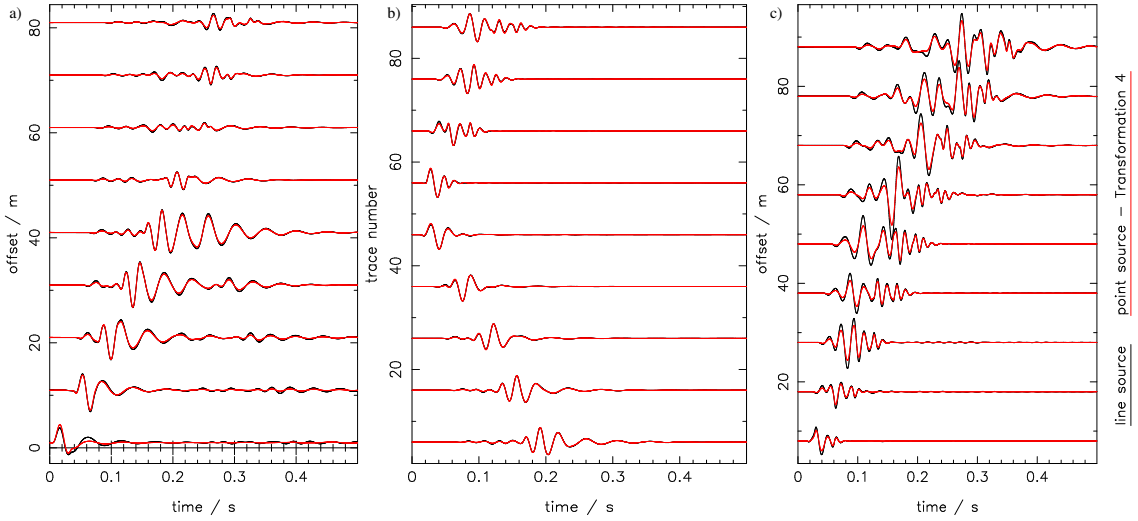

Figure 5: Transformation 4 - Single Velocity Transformation. Comparison of line source seismograms (black) and corrected point source seismograms (red) (vertical component) for the true model in Figure 7a); not all traces are shown. Seismogram a) shows a shot at 5 m distance (very left part of the model), seismogram b) a shot at 50 m distance (middle of the model) and seismogram c) a shot at 94 m distance (very right part of the model). The seismograms in a) and c) are not trace normalized but scaled by an offset dependent factor $\left(\frac{r}{1\,\mathrm{m}}\right)^{0.3}$ to equalize plot scale amplitudes. The seismogram b) is trace normalized, please notice that the y-axis is the trace number not the offset in this case.

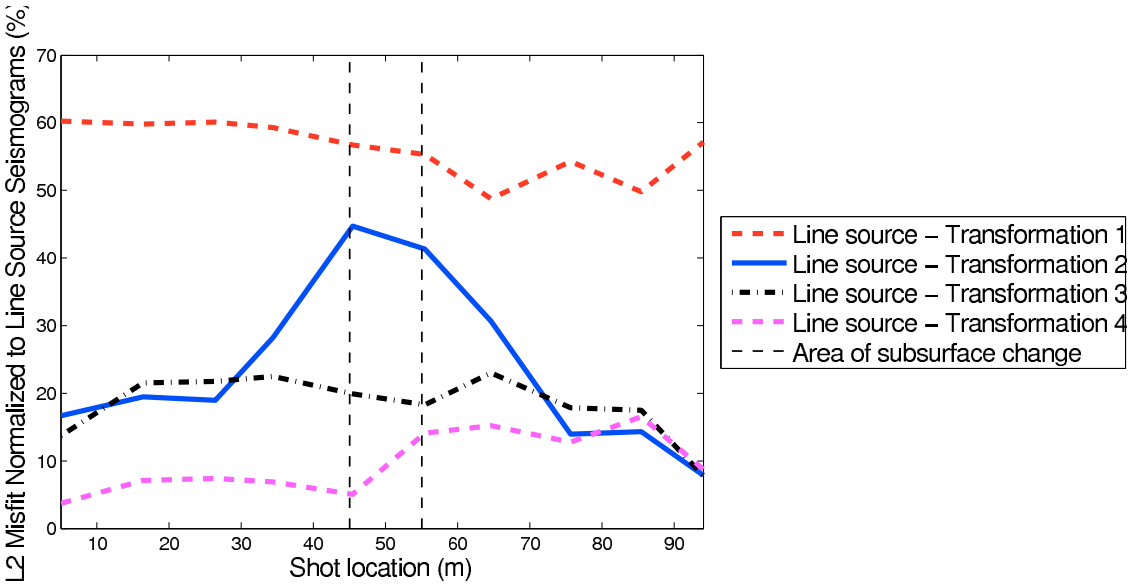

Figure 6: L2 norm misfit trend with shot location. Area of thin dashed lines indicates the location of the step in the layer of the subsurface model (see Figure 7a)).

APPLICATION OF FULL WAVEFORM INVERSION FOR SHALLOW SEISMIC SURFACE WAVES

Before we present and discuss our inversion results, we briefly introduce our inversion parameters and strategies during our FWI investigations. The aim of the full waveform inversion is to minimize the objective function (Mora (1987), Tarantola (1986))

$$E_{L2norm} = \sum_i \sum_j \|\boldsymbol{u}_{i,j} - \boldsymbol{d}_{i,j}\|^2 \tag{9}$$

which is the signal energy of residuals between the modeled data **u** and observed data **d** to infer the material parameters **m** in the subsurface model. The indexes i and j indicate the sources and receivers, respectively. We are using an iterative steepest-descend gradient method to update the model parameters $\boldsymbol{m}_n$ at iteration step *n* (Köhn, 2011)

$$m_{n+1} = m_n - \mu_n P_n \left(\frac{\partial E}{\partial m}\right)_n , \tag{10}$$

where $\left(\frac{\partial E}{\partial m}\right)_n$ denotes the gradient direction of the objective function with respect to the model parameters, P_n an appropriate preconditioning operator and μ_n the step length. The gradients can be expressed by a zero-lag correlation of displacment wavefields (Mora (1987), Tarantola (1986) and Köhn (2011)). To increase the convergence speed we use the conjugate gradient direction (Mora, 1987) and preconditioning of the gradients with the Pseudo-Hessian matrix (Sheen et al., 2006). Furthermore, we taper shotwise the gradients circular at the source locations to avoid strong artifacts. The model parameters are the S-velocity, the P-velocity and the density (Köhn et al., 2012). For the force time function we use the first period of a $\sin^3(t)$ with a frequency bandwidth of 0 Hz to about 100 Hz. Since the source wavelet is known, it is not estimated during inversion. Furthermore, we use a multistage approach for inversion with frequency filtering to reduce the nonlinearity of the misfit function (Sirgue and Pratt, 2004). Starting at low frequencies builds up a smooth subsurface model and prevents the FWI to end up in a local minimum. We start at a low pass frequency of 10 Hz and increase the range of frequencies in steps of 10 Hz up to the full bandwidth of the source signal.

In Figure 7a) the true subsurface model is displayed. It is characterized by a layer with a step over halfspace, whereat the layer and halfspace is not completely homogenous, but has a smooth gradient especially at the transition zone of layer and halfspace. The used velocities and density range is realistic for shallow seismic subsurface. For all investigations we use initial models constructed with linear gradients as shown in Figure 7b). As sources we applied 20 vertical point forces resembling hammer blows and recorded the wavefields with 88 receivers (horizontal and vertical component) with spacing of 1 m. All test cases are synthetic data (true subsurface model is known) and can be called reconstruction tests.

Reference FWI result - perfect line source seismograms

To evaluate a reference FWI result we use perfect line source seismograms as observed data during inversion. The objective is to learn more about the inversion procedure and the resolution power by using surface waves. Furthermore, there is no error by applying a transformation technique. Hence, all FWI results in the next section have to be compared with this reference FWI result.

In Figure 7a) and b) the true subsurface and starting models are plotted. The comparison of the seismograms of the true and starting model are shown in Figure 7c) for an exemplary shot at 5 m distance. The velocities and density values in the very shallow are in the same range, but the seismogram of the starting model is completely 1D whereas the seismogram of the true subsurface contains a change in the dispersion and reflected waves of the step in the layer. In Figures 7d)-f) the FWI results of the S-velocity, P-velocity and Density, respectively, are plotted with the same colorbar as in a) and b). The seismograms in Figure 7 g) show the comparison of the seismogram of the true subsurface and the seismogram of the inverted model. We observe a very good fit in this comparison. Judging from the waveform only we apparently have estimated an appropriate subsurface model during inversion. For the final seismograms in the FWI we obtain L2 norm misfit of 2.75 %. We obtain satisfatory subsurface models in Figure 7d)-f), however, also some less resolution like underestimated halfspace values due to the insufficient penetration depth of the

Rayleigh wave with the dominant wave length and a smoother transition zone than in the true model. The S-velocity model has a much higher resolution than the P-velocity and Density model because of the high sensitivity of surface waves to the S-velocity. Nevertheless, it is possible to obtain a reliable 2D subsurface model with a 1D starting model by using FWI with shallow seismic surface waves.

Reconstruction tests for corrected point source seismograms

In this section we discuss 2D FWI results with point source seismograms as observed data which were corrected with different 3D/2D transformation techniques. Due to the high sensitivity of surface waves to the S-velocity we present only the S-velocity models to investigate the effects of geometrical spreading corrections towards a FWI with surface waves. To help clarifying the different inversion results we show only investigations for Transformation 1-3, because the Single Velocity Transformation produces almost the same inversion result as the Direct Wave Transformation.

First of all we would like to mention that all inversion tests run with the same parameter settings like frequency filtering, starting models and so on as for the reference inversion in the previous section. We obtain L2 norm misfits for the final seismograms in the FWI between 14.03 $\%$ for the Direct Wave Transformation, 18.85 $\%$ for the Amplitude-only Transformation and 82.21 $\%$ for the Fourier-Bessel Transformation (Table 9 - first line). If we consider on the one hand the L2 norm as a measure of how succesful an inversion is, it is clear that the inversion of the Direct Wave and the Amplitude-only Transformation should be more reliabe than the inversion of the Fourier-Bessel Transformation. However, on the other hand it is essential how well the inversion could reconstruct the subsurface model. In Figure 8b)-d) the inversion results with corrected point source seismograms as observed data are plotted and in Figure 8a) again the reference inversion result with line source seismograms as observed data. A single value appears to be insufficient to describe the inversion results completely. Because of this we display in Figure 8e)-h) a relative error between the true und the inverted S-velocity model

$$\text{relative error}(x,z) = \frac{m_{true}(x,z) - m_{syn}(x,z)}{m_{true}(x,z)} \tag{11}$$

where x and z indicate the spatial coordinates, m_{true} the true subsurface and m_{syn} the inverted model. At first view the inversion results with the Amplitude-only and the Direct Wave Transformation seem to be similar and comparable with the reference inversion result. The inversion result for the Fourier-Bessel Transformation significantly shows less resolution. Nevertheless, all inversion tests minimize the L2 norm with different observed data why it is clear that the differences must be in some details. For the reference inversion result in Figure 8a) and e), it is obvious that the velocities in the halfspace for the right part of the model are underestimated and that mainly the transition zone between the layer and the halfspace is overestimated. So we have to keep that in mind and cannot expect a better resolution to the inversions with corrected point source seismograms. It is conspicuous that the inversion with the Amplitude-only Transformation carves out a significant to high velocity area above the transition zone. We guess this is probably due to the disregarded phase delay correction. The inversion of the Direct Wave Transformation can be considered as the most reliable reconstruction in comparison to the reference inversion result. However, we obtain an artifact at the step of the layer as a result of the small amplitudes of the reflected surface waves due to the taper with $t^{-1/2}$ of the transformation. The relative error in Figure 8h) for the inversion with the Fourier-Bessel Transformation is quite high in the entire model. This was expectable with the experience of Section '3D/2D Transformation Techniques for shallow seismic surface waves' as Transformation 2 is not able to reproduce a 2D wavefield.

A final consideration will emphasize our discussion. Normally we would do a 3D modelling on the inverted models to obtain 3D wavefields and compare them to the originally observed 3D wavefields to close the circle. But to save computional time we do it the other way around and simply calculate the L2 norm between the final seismograms of each inversion and line source seismograms of the true subsurface model (Table 9 - third line). It is clear that the misfit value for line source seismograms is the same as in the end of the inversion. But for the three inversions with point source seismograms as observed data we are able to infer the quality of the reconstruction of the model from the different transformation techniques. The not-explained energy in the residuals of the Amplitude-only and the Fourier-Bessel Transformation is over 50 $\%$ whereas the L2 norm for the Direct Wave Transformation amounts around 18 $\%$. For sure in

comparison to the reference line source inversion it is quite high but much less than for the other 3D/2D correction filters.

CONCLUSIONS

With the objective to realize a 2D full waveform inversion of field data, we have to deal with the different spreading of recorded and computed waves. In the first part of the paper we have discussed four different 3D/2D transfomation techniques. One of them uses a wave-theoretical approach which requires a complete common source gather and the other transformation techniques have the benefit of being applicable to individual traces. The most appropriate correction filter is the Direct Wave Transformation after Forbriger et al. (2012) as it is applicable to 2D structures and single traces and it corrects both the amplitude-decay as well as the phase delay.

In the second part of the paper we have investigated line source and corrected point source seismograms as observed data. The FWI with shallow seismic surface waves has the potential to reconstruct the subsurface reliably. The L2 norm is remarkable minimized to 2.75 $\%$ by using line source seismograms. When using the L2 norm as a measure of misfit a correction for the different decay of amplitudes is mandatory but not sufficient to obtain reliable inversion results. In addition the signal phase must also be corrected which should be done with the most appropriate physical accuracy. On account of this we should not apply the Fourier-Bessel Transformation, because it is only valid for 1D structures. Hence we propose to use the Direct Wave Transformation which is the most appropriate 3D/2D transformation technique for shallow seismic surface waves we have tested so far.

ACKNOWLEDGMENTS

The work was performed within the GEOTECHNOLOGIEN program, funded by the German Ministry of Education and Research (BMBF) and German Research Foundation (DFG), Grant 03G0752. It was also kindly supported by the sponsors of the *Wave Inversion Technology (WIT) Consortium*, Germany.

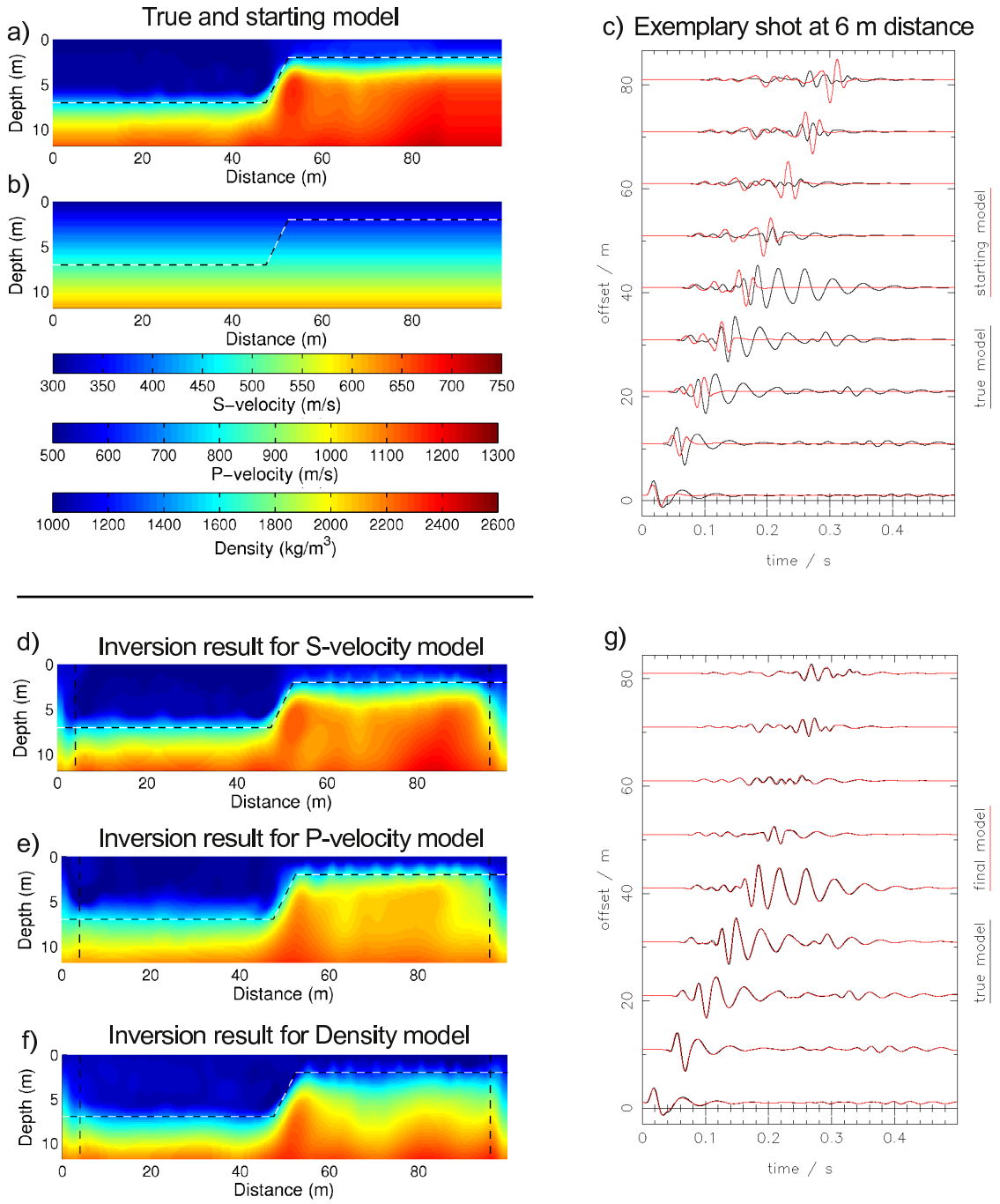

Figure 7: The true and starting model is shown in a) and b), respectively. Seismogram c) shows the wavefields of a shot at 5 m distance (very left part of the model) for the true (black line) and the starting (red line) model. FWI results of S-velocity, P-velocity and Density model are plotted in d)-f), respectively, with perfect line source seismograms (subfigure c)) as observed data. The black/white dashed line indicates the transition zone of layer and halfspace in the true subsurface model. The absorbing boundary with perfectly matched layers (CPML) is plotted with black dashed lines. Seismograms g) show the waves of a shot at 5 m distance (very left part of the model) of the true (black line) and final (red line) model after inversion.

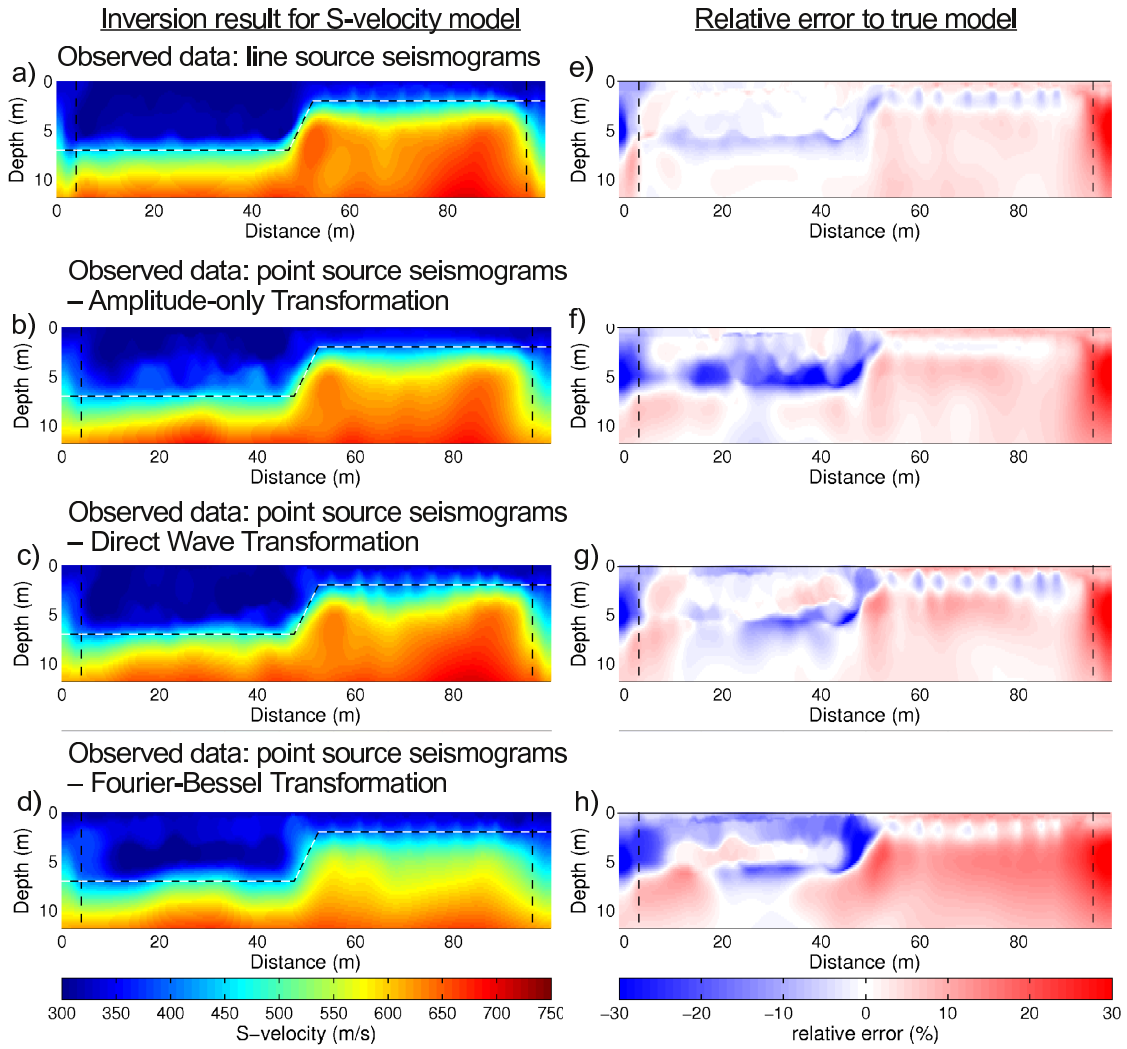

Figure 8: FWI results for line source and corrected point source seismograms as observed data in a)-d) and relative error to true subsurface model in e)-h). The black/white dashed line indicates the transition zone between layer and halfspace in the true subsurface model. The absorbing boundary with perfectly matched layers (CPML) is plotted with black dashed lines.

Observed data in FWI:	line source seismograms	point source seismograms Amplitude-only Transformation	point source seismograms Direct Wave Transformation	point source seismograms Founier-Bessel Transformation
Final data misfit in FWI	2.75 %	18.85 %	14.03 %	82.21 %
Number of iterations	206	132	133	122
Duration with 8 CPUs	22.6 h	12.7 h	11.8 h	14.1 h
Data misfit for final model with respect to reference seismograms	2.75 %	51.05 %	17.96 %	50.14 %

Figure 9: Final L2 data misfit in the end of the full waveform inversion for different observed data and the number of iterations. Furthermore the L2 data misfit between final seismograms and true line source seismograms. The horizontal and vertical component are considered for this calculation.

REFERENCES

Amundsen, L. and Reitan, A. (1994). Transformation from 2-D to 3-D wave propagation for horizontally layered media. *Geophysics*, 59(12):1920–1926.

Bohlen, T. (2002). Parallel 3-D viscoelastic finite difference seismic modelling. *Computers & Geosciences*, 28:887–899.

Crase, E., Pica, A., Noble, M., McDonald, J., and Tarantola, A. (1990). Robust elastic nonlinear waveform inversion: Application to real data. *Geophysics*, 55(5):527–538.

Dunkl, S., Kurzmann, A., and Bohlen, T. (2012). 3d elastic full waveform inversion of small-scale heterogeneities in transmission geometry. *Geophysical Prospecting*, Submitted Sept. 2012.

Forbriger, T. (2003). Inversion of shallow-seismic wavefields: Part I and II. *Geophys. J. Int.*, 153(3):719–752.

Forbriger, T., Groos, L., and Schäfer, M. (2012). Appropriate line source simulation procedure for shallow seismic field data. *Geophys. J. Int.*, in preperation.

Köhn, D. (2011). Time domain 2D elastic full waveform tomography. *Ph.D. thesis, Christian-Albrechts-Universität zu Kiel*.

Köhn, D., De Nil, D., Kurzmann, A., Przebindowska, A., and Bohlen, T. (2012). On the influence of model parametrization in elastic full waveform tomography. *Geophys. J. Int.*, 191(1):325–345.

Mora, P. (1987). Nonlinear two-dimensional elastic inversion of multioffset seismi data. *Geophysics*, 55(3):1211–1228.

Pica, A., Diet, J., and Tarantola, A. (1990). Nonlinear inversion of seismic reflection data in a laterally invariant medium. *Geophysics*, 55(3):284–292.

Romdhane, G., Grandjean, G., Brossier, R., Rejiba, F., Operto, S., and Virieux, J. (2011). Shallow-structure characterization by 2D elastic full-waveform inversion. *Geophysics*, 76(3):R81–R93.

Sheen, D.-H., Tuncay, K., Baag, C.-E., and Ortoleva, P. J. (2006). Time domain gauss-newton seismic waveform inversion in elastic media. *Geophys. J. Int.*, 167(3):1373–1384.

Sirgue, L. and Pratt, R. G. (2004). Efficient waveform inversion and imaging: A strategy for selecting temporal frequencies. *Geophysics*, 69(1):231–248.

Tarantola, A. (1986). A strategy for linearized elastic inversion of seismic reflection data. *Geophysics*, 51:1893–1903.

Tran, K. T. and McVay, M. (2012). Site characterization using gauss newton inversion of 2-D full seismic waveform in the time domain. *Soil Dynamics and Earthquake Engineering*, 43:16–24.

Wapenaar, C., Verschuur, D., and Herrmann, P. (1992). Amplitude preprocessing of single and multicomponent seismic data. *Geophysics*, 57(9):1178–1188.